PNAS RESEARCH ARTICLE | BIOCHEMISTRY

Sequential absorption of two photons creates a bistable form of RubyACR responsible for its strong desensitization

Oleg A. Sineshchekov[a], Elena G. Govorunova[a], Hai Li[a], Yumei Wang[a], and John L. Spudich[a,1]

Edited by Adam E. Cohen, Harvard University, Cambridge, MA; received January 27, 2023; accepted April 18, 2023 by Editorial Board Member Jeremy Nathans

Channelrhodopsins with red-shifted absorption, rare in nature, are highly desired for optogenetics because light of longer wavelengths more deeply penetrates biological tissue. RubyACRs (Anion ChannelRhodopsins), a group of four closely related anion-conducting channelrhodopsins from thraustochytrid protists, are the most red-shifted channelrhodopsins known with absorption maxima up to 610 nm. Their photocurrents are large, as is typical of blue- and green-absorbing ACRs, but they rapidly decrease during continuous illumination (desensitization) and extremely slowly recover in the dark. Here, we show that long-lasting desensitization of RubyACRs results from photochemistry not observed in any previously studied channelrhodopsins. Absorption of a second photon by a photocycle intermediate with maximal absorption at 640 nm (P_{640}) renders RubyACR bistable (i.e., very slowly interconvertible between two spectrally distinct forms). The photocycle of this bistable form involves long-lived nonconducting states (L_{long} and M_{long}), formation of which is the reason for long-lasting desensitization of RubyACR photocurrents. Both L_{long} and M_{long} are photoactive and convert to the initial unphotolyzed state upon blue or ultraviolet (UV) illumination, respectively. We show that desensitization of RubyACRs can be reduced or even eliminated by using ns laser flashes, trains of short light pulses instead of continuous illumination to avoid formation of L_{long} and M_{long}, or by application of pulses of blue light between pulses of red light to photoconvert L_{long} to the initial unphotolyzed state.

channelrhodopsins | optogenetics | retinal proteins | photochemistry

Significance

Optogenetic control of neuronal activity requires tools that absorb deeper penetrating red light. Anion-conducting channelrhodopsins known as RubyACRs (Anion ChannelRhodopsins) are the most red-shifted channelrhodopsins to date. They generate large passive currents but show rapid and long-lasting desensitization, which compromises their utility as optogenetic silencers. This study reveals the photochemical mechanism of RubyACR desensitization not previously described for any other channelrhodopsin.

Anion channelrhodopsins (ACRs) are light-gated anion channels found in protists of several major phylogenetic lineages, including cryptophytes, haptophytes, and stramenopiles (1). When expressed in mature neurons or cardiomyocytes, ACRs enable temporally precise membrane hyperpolarization and inhibition of action potential generation (2, 3). ACRs have been successfully used for neuronal silencing and behavioral control in worms (4), flies (5), zebrafish (6), mice (7), rats (8), ferrets (9), and nonhuman primates (10), and for control of plant growth (11). Moreover, ACRs are considered for optogenetic treatment of chronic pain (12) and cardiac defibrillation (13) in human patients. However, most of ~200 currently known natural ACRs primarily absorb blue or green light that is strongly scattered by biological tissues. Four closely related thraustochytrid ACRs known as RubyACRs are exceptional in that they exhibit strongly red-shifted spectral sensitivity with maxima at 590 to 610 nm (14) and thus are particularly promising for optogenetic applications. ACR1 from *Hondaea fermentalgiana* (*Hf*ACR1) generates the largest photocurrents of the known RubyACRs. Under illumination with continuous red light, *Hf*ACR1 photocurrents rapidly decrease to a lower steady-state level (i.e., exhibit desensitization). Unlike other channelrhodopsins (ChRs), desensitized photocurrents in RubyACRs do not recover even after many minutes in darkness, which suggests a unique mechanism. Better understanding of this mechanism is needed to devise protocols to eliminate desensitization of RubyACRs in optogenetic experiments.

All microbial rhodopsins, except enzymerhodopsins that have an additional N-terminal helix, contain seven transmembrane helices that form a retinylidene photoactive domain similar to their counterparts responsible for vision in animals (15–18). Retinal is attached to a conserved Lys residue in the 7th helix via a Schiff base linkage that in most rhodopsins is protonated in the unphotolyzed state. Upon photoexcitation, microbial rhodopsins undergo a cycle of photochemical conversions that result in restoration of the initial state. Spectrally distinct intermediates of the photocycle are usually designated by the letters K, L, M, N, and O (19), following the tradition initiated by research in bacteriorhodopsin, the first discovered microbial rhodopsin. Photoinduced isomerization of all-*trans*-retinal to its 13-*cis* form (formation of the K intermediate) is followed by a series of thermal relaxations; a spectrally dominant process is deprotonation and subsequent reprotonation of the Schiff base (formation and dissipation of the blue-shifted M intermediate, respectively). Temporal

Author affiliations: [a]Department of Biochemistry and Molecular Biology, Center for Membrane Biology, The University of Texas Health Science Center at Houston McGovern Medical School, Houston, TX 77030

Author contributions: O.A.S., E.G.G., and J.L.S. designed research; O.A.S., E.G.G., H.L., and Y.W. performed research; O.A.S. and E.G.G. analyzed data; and O.A.S., E.G.G., and J.L.S. wrote the paper.

The authors declare no competing interest.

This article is a PNAS Direct Submission. A.E.C. is a guest editor invited by the Editorial Board.

[1]To whom correspondence may be addressed. Email: John.L.Spudich@uth.tmc.edu.

This article contains supporting information online at https://www.pnas.org/lookup/suppl/doi:10.1073/pnas.2301521120/-/DCSupplemental.

Published May 15, 2023.

correlation between individual photocycle intermediates and channel states is different in different types of ChRs. In particular, in cryptophyte ACRs, deprotonation of the Schiff base (formation of the M intermediate) correlates with an early phase of channel closing (20), whereas in chlorophyte cation channelrhodopsins, M formation predates channel opening (21).

Desensitization, a decrease in current amplitude common to ChRs in continuous light, results from the accumulation of nonconductive or poorly conductive photocycle intermediates, which appear to be different in different ChRs (22–25). Here, we carry out a comparative analysis of absorption changes in nondenaturing detergent-purified *Hf*ACR1 and photocurrents generated by this RubyACR channel in biological membranes. We found that under continuous illumination, absorption of a second photon by a specific photocycle intermediate leads to the formation of extremely long-lived bistable states responsible for desensitization. Based on our results, we propose guidelines for the design of illumination protocols that would exclude desensitization and facilitate efficient use of RubyACRs for neuronal silencing.

Results

Absorption Spectroscopy of Purified *Hf*ACR1. The initial dark-adapted form of purified *Hf*ACR1 showed maximal absorption (λ_{max}) at ~590 nm (Fig. 1*A*, black line). The blue shift of the absorption maximum compared to that of the action spectrum of photoelectric responses [610 nm (14)] can be explained by the effect of detergent and possibly contribution of a small fraction of a nonphotoactive 13-*cis* retinal-bound form. Illumination at λ_{max} caused disappearance of the main band in parallel with the appearance of a strongly blue-shifted form (Fig. 1*A*, red line). The maximum of the difference (light-minus-dark) spectrum was at 465 nm with a small shoulder at <400 nm (Fig. 1*B*). In the dark, the blue-absorbing form slowly converted to an ultraviolet (UV)-absorbing product (Fig. 1*A*, gray line) with the maximum of the difference spectrum at ~380 nm (Fig. 1*C*). The time constant (τ) of this dark transition was >1 h (Fig. 1*D*). Even after 14 h in darkness, only a small fraction of the initial red-absorbing form was recovered (Fig. 1*C*, red line). Based on the relative positions of their λ_{max} values and the sequence of their appearance, we conclude that the blue form represents a long-lived L-like intermediate of the photocycle (L_{long}), and the UV form, a long-lived M-like intermediate (M_{long}).

Illumination of the red light-adapted form with blue (490 nm) light recovered the initial unphotolyzed state (Fig. 1*E*). This recovery was incomplete (Fig. 1*E*, blue line), as expected because blue light was absorbed not only by L_{long}, but also by the unphotolyzed state. In contrast, conversion from the unphotolyzed state to L_{long} was more complete, since L_{long} practically does not absorb red light, because the long-wavelength slope of the absorption spectrum of the pigment is steeper than the short-wavelength slope. The difference (light minus dark) spectrum of the recovery of the initial state from L_{long} is shown in Fig. 1*F* (blue line). The M_{long} could also be photoconverted to the initial state upon illumination with UV light (Fig. 1*F*, black line).

Photocurrents in HEK293 (Human Embryonic Kidney) Cells under Continuous and Pulsed Illumination. To mimic the ionic conditions of mature neurons, we carried out whole-cell patch clamp measurements using the pipette and bath solutions containing 4 and 130 mM Cl^-, respectively (for the full compositions, see *Materials and Methods*). In agreement with depletion of the unphotolyzed state form in the purified protein, illumination with red light caused strong long-lasting desensitization of photocurrent that did not recover even when 2-s light pulses were applied with 30-s dark intervals (Fig. 2 *A*, *Upper Row* of traces). After three light pulses, the photocurrent reduced

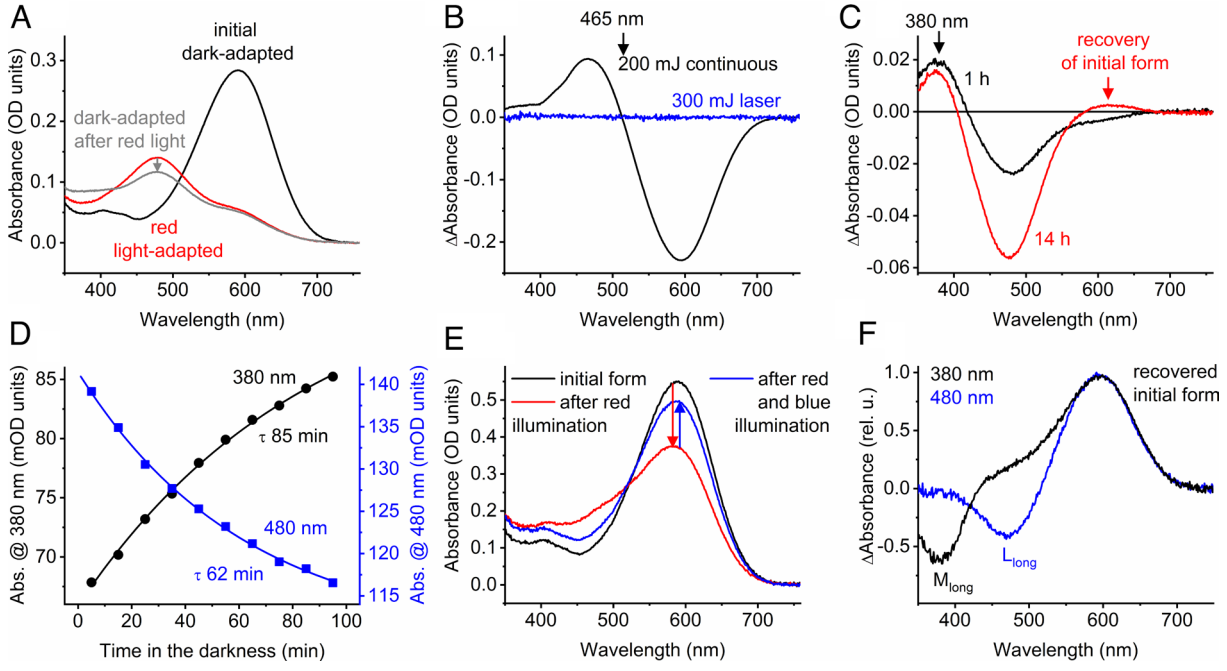

Fig. 1. Absorption spectroscopy of purified *Hf*ACR1. (*A*) Absorption spectra of the initial dark-adapted detergent-purified protein (black), the same sample after continuous illumination with red light (600 ± 10 nm, 3.3 mW cm^{-2} for 60 s, red), and the same sample after subsequent 95-min dark adaptation (gray). (*B*) The light-minus-dark difference spectra after continuous illumination (Fig. 1*A*) or 75 laser flashes (532 nm, 6-ns, 5 mJ, 0.1 Hz; blue). Doses applied to the sample are indicated in the figure. (*C*) The dark-minus-light difference spectra of the red light–illuminated sample measured after 1 h (black) and 14 h in the dark (red). (*D*) The dependence of absorbance at 380 nm (*Left* axis, black) and 480 nm (*Right* axis, blue) on the time of dark adaptation of red light–illuminated protein. (*E*) Absorption spectra of initial dark-adapted protein (black), the same sample after illumination with red light (3.3 mW cm^{-2} for 25 s, red), and after subsequent illumination with blue light (500 ± 10 nm, 2.8 mW cm^{-2} for 60 s, blue). (*F*) Absorption difference spectra of red light–adapted protein illuminated with 380-nm (black) or 480-nm (blue) light.

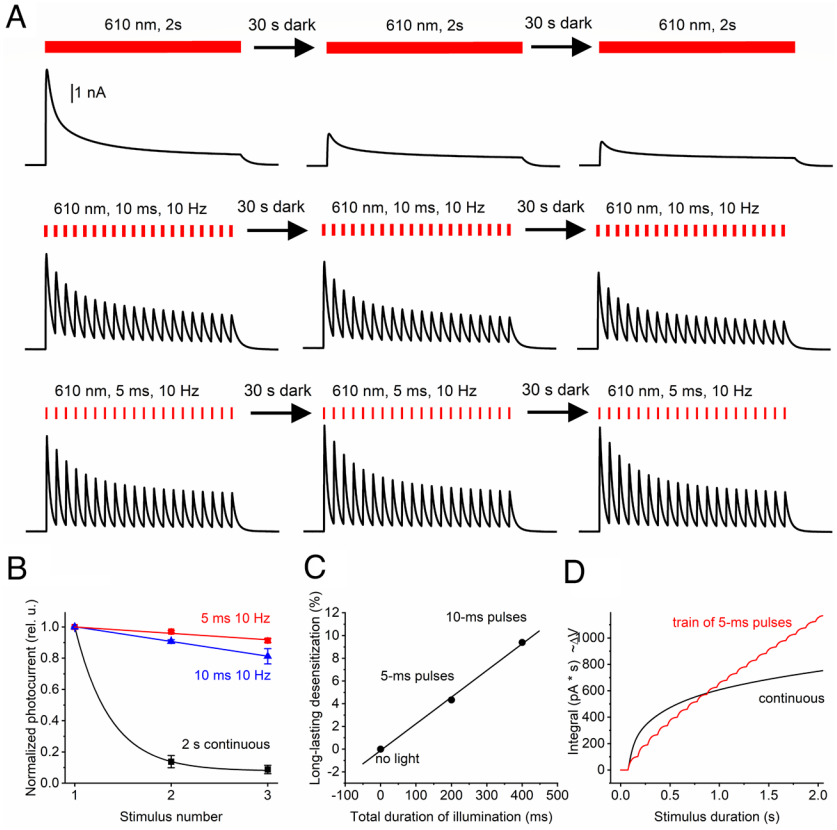

Fig. 2. Photocurrents under continuous and pulsed illumination. (*A*) Photocurrent traces recorded in response to three subsequent pulses of continuous 2-s light (*Upper Row*); three 10-Hz trains of 10-ms pulses (*Middle Row*); and three 10-Hz trains of 5-ms pulses (*Bottom Row*). The red bars show the timing of illumination. (*B*) Mean photocurrent elicited by the 2nd and 3rd 2-s stimulus (continuous or pulsed) normalized to that elicited by the 1st stimulus. The symbols are the mean values ± SEM, n = 3 cells. (*C*) The dependence of desensitization on the total duration of illumination (the 1st and 2nd stimuli combined). (*D*) The dependence of the integral under the photocurrent trace on the duration of illumination upon continuous (black) or pulsed (red) stimulation.

10-fold (Fig. 2*B*, black), which was consistent with nearly total disappearance of the unphotolyzed red-absorbing form of purified protein after strong red illumination (Fig. 1*A*).

When trains of short (5- or 10-ms) light pulses at 10-Hz frequency were applied instead of 2-s periods of continuous illumination, photocurrent decrease was much smaller (Fig. 2 *A*, *Middle* and *Bottom Rows* of traces). Photocurrent decrease was proportional to the dose of light (Fig. 2 *B* and *C*), which means that the target of the second quantum appeared in <5 ms. Suppression of neuronal activity depends on the extent of membrane hyperpolarization that is proportional to the number of charges transported across the membrane. After 1 s, the number of charges (calculated as the integral under the photocurrent curve) during a train of 5-ms pulses exceeded that under continuous light (Fig. 2*D*), which means that neuronal silencing under pulsed illumination would be more efficient than that under continuous light, when photocurrent decrease during the train of pulses is an order of magnitude lower than under the continuous light (Fig. 2*A*).

When 2-s pulses of red light were applied with 2-s dark intervals (Fig. 3 *A*, *Left* part), both peak photocurrent and the integral (proportional to membrane hyperpolarization) decreased almost to zero after the third pulse (Fig. 3 *C* and *D*, red open circles). However, when blue light pulses were applied between the red-light pulses (Fig. 3 *A*, *Right* part), the response to the second and subsequent red-light pulses was 30-fold larger than that without blue preillumination (Fig. 3 *C* and *D*, red filled circles). This behavior was in full agreement with photorecovery of the unphotolyzed state from L_{long} upon blue light illumination (Fig. 1 *E* and *F*). The photocurrent recovery after a blue light pulse was not complete, like that in experiments with blue illumination of the purified protein (Fig. 1*E* and its explanation in the text).

Blue light pulses applied between red pulses also produced photocurrents (Fig. 3 *A*, *Right* part). Comparison of the current kinetics in response to a blue pulse (applied after a red pulse) and a red pulse (applied after a blue pulse) is shown in Fig. 3*B*. In response to blue light, both components of the current rise were ~sixfold slower, and, most importantly, the two components of desensitization were 10- and 20-fold slower than in response to red light. Consequently, the number of charges transported across the membrane during the blue pulse (and hence the change in the membrane potential) was almost 2 orders of magnitude larger than that in response to the second and subsequent red pulses (Fig. 3*D*, blue solid squares and red open circles, respectively).

Mechanism of Desensitization and Characterization of the Target of Second Photon. Continuous red light led to strong depletion of the unphotolyzed form (Fig. 1*B*) and a corresponding decrease in photocurrent (Fig. 2 *A*, *Upper Row*). However, when the same or a higher number of quanta were delivered to the sample in the form of 6-ns laser flashes, no long-lasting absorption changes (Fig. 1*B*, blue line) and no decrease in the amplitude of photocurrent (see below) were observed if the time interval between the flashes was >10 s (Fig. 1*B*, blue line). This means that absorption of the second photon only during the photocycle transforms *Hf*ACR1 to a bistable pigment.

To determine the lifetime of the target, we progressively shortened the interval between laser flashes. This led to the appearance of a typical difference signal with a negative red band and a positive blue band (Fig. 4*A*), like that observed under continuous illumination (Fig. 1*B*, black line). The saturation constant of peak-to-peak amplitude of difference was ~10 Hz (Fig. 4*B*), which means that the lifetime of the target of the second photon absorption was ~100 ms.

To estimate the spectral characteristics of the target of the second photon, we analyzed the spectral dependence of desensitization. The maximum of the desensitization action spectrum was 625 nm, i.e., 15 nm red-shifted as compared to the action spectrum of the photocurrent (Fig. 4*C*). However, the efficiency of

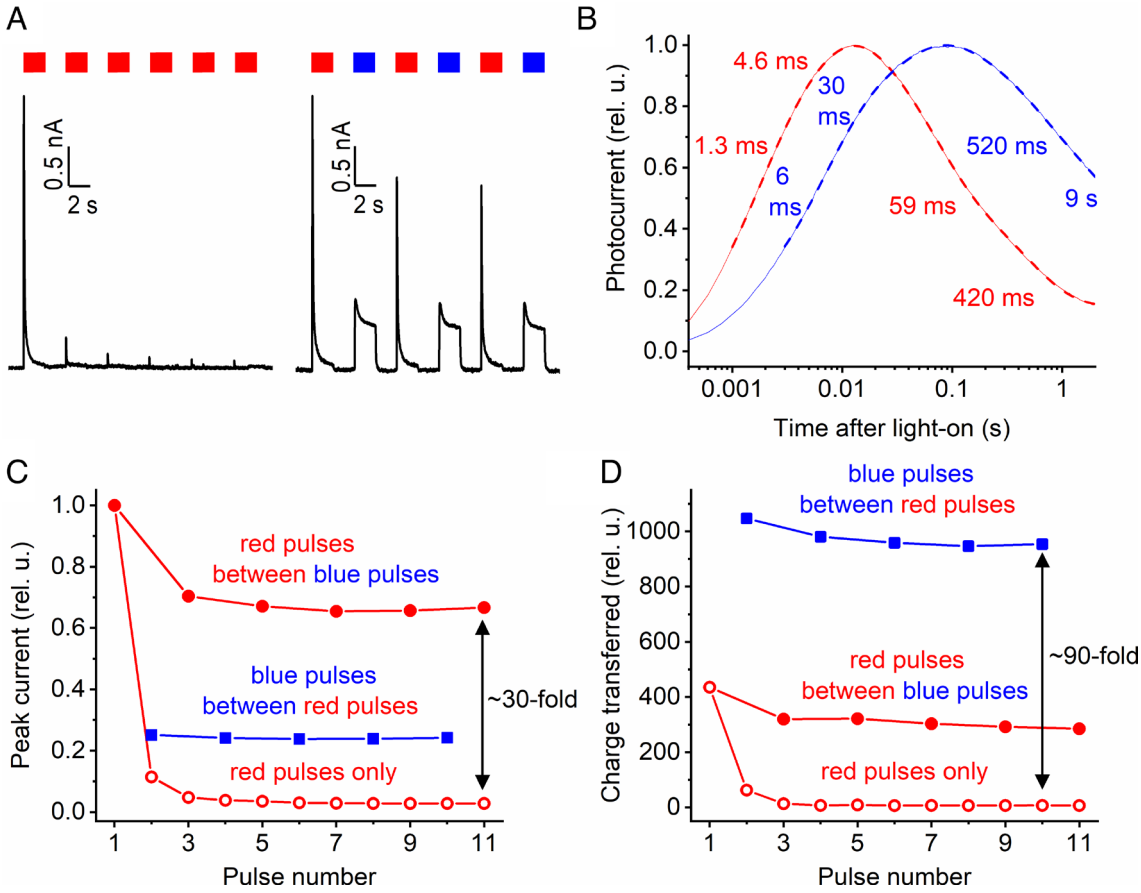

Fig. 3. Recovery of red light–induced photocurrents by blue light. (*A*) Photocurrent traces in response to 2-s pulses of red or blue light, the timing of which is shown on *Top*. *Left*, only red pulses were applied; *Right*, the red pulses were interspersed with blue pulses. (*B*) Red- or blue-light-evoked photocurrent traces on the expanded time scale. (*C* and *D*) Peak photocurrent normalized to that in response to the first light pulse (*C*) or integral (*D*) measured upon illumination with red light pulses (red open circles), red pulses between blue pulses (red filled circles), and blue pulses between red pulses (blue squares).

desensitization must also depend on the absorption of the initial unphotolyzed form that converts to the target of the second photon, which means that the actual absorption of the target peaks at a more red-shifted value. This conclusion was confirmed by measurement of the action spectrum of the disappearance of the initial unphotolyzed state in the purified protein. The red shift of this action spectrum from the absorption spectrum of purified protein was even larger (*SI Appendix*, Fig. S1*A*).

To clarify spectral and kinetic characteristics of the target of the second photon and other intermediates of the single-turnover photocycle, we measured flash-induced absorbance changes in response to 6-ns laser flashes at 0.05 Hz frequency to avoid formation of long-lived products by two-photon absorption (*SI Appendix*, Fig. S2). The fastest component of the global fit analysis appeared with τ ~4 µs and revealed a red-shifted intermediate with an absorption maximum of 640 nm, which we named P_{640} (Fig. 4*D*, red symbols and line). To follow the kinetics of this intermediate, we subtracted absorption change kinetics recorded at 600 nm from that at 640 nm. Consistent with the results of global fit analysis, P_{640} was generated in ~3 µs (Fig. 4*E*) and remained stable for ~100 ms (Fig. 4*B*). We conclude that it is the target of second photon absorption leading to generation of L_{long}.

Typical of other retinal proteins, L-like and M-like intermediates were also revealed by our global fit analysis (Fig. 4*D*, blue). The L-like intermediate (observed at 480 nm) accumulated with 3-exponential kinetics (Fig. 4*F*). The main accumulation (3/4 of the full amplitude) took place with τ ~1 to 2 µs in parallel with depletion of the red-shifted K intermediate (*SI Appendix*, Fig. S3). The M intermediate appears with τ ~3.8 ms (*SI Appendix*, Fig. S4), which should correspond to the τ of fast L decay. However, absorption at 480 nm continues to rise and decays very slowly (Fig. 4*F*). This can be due to fast generation of an N-like intermediate absorbing in the same range. In contrast to most other microbial rhodopsins, only a small amount of the M intermediate accumulated in *Hf*ACR1 (<3% of the amount of the photoconverted initial form). The rate of M accumulation was slow (τ 3.8 ms, *SI Appendix*, Fig. S4), as in cryptophyte ACRs (20).

Photocurrents Evoked by Laser Flash Excitation. A series of *Hf*ACR1 photocurrent traces evoked by laser flash excitation at different holding voltages (V_h) is shown in Fig. 5*A*. The reversal potential (V_r) of the peak current was 79 ± 2 mV (n = 4 cells) (*SI Appendix*, Fig. S5). Four exponential components were required to fit the current trace: three for channel opening and one for closing (*SI Appendix*, Fig. S6). But, a small-amplitude slowest opening component (τ in the ms range) could only be observed at the voltages more positive than the reversal potential, and a component with τ ~0.4 ms was not more than 3% of the full amplitude. Therefore, the channel kinetics of major changes could be described as two-exponential: the rise and decay of current. The additional decay component observed in other ACRs (14, 26) could not be clearly resolved.

The V_r of the fast opening of the channel was shifted ~10 mV to negative values from that of the slower components and peak current (*SI Appendix*, Fig. S6). This can be explained by the existence of a fast unresolved negative current, which is evident at voltages near V_r (Fig. 5*B*). This current component is essentially

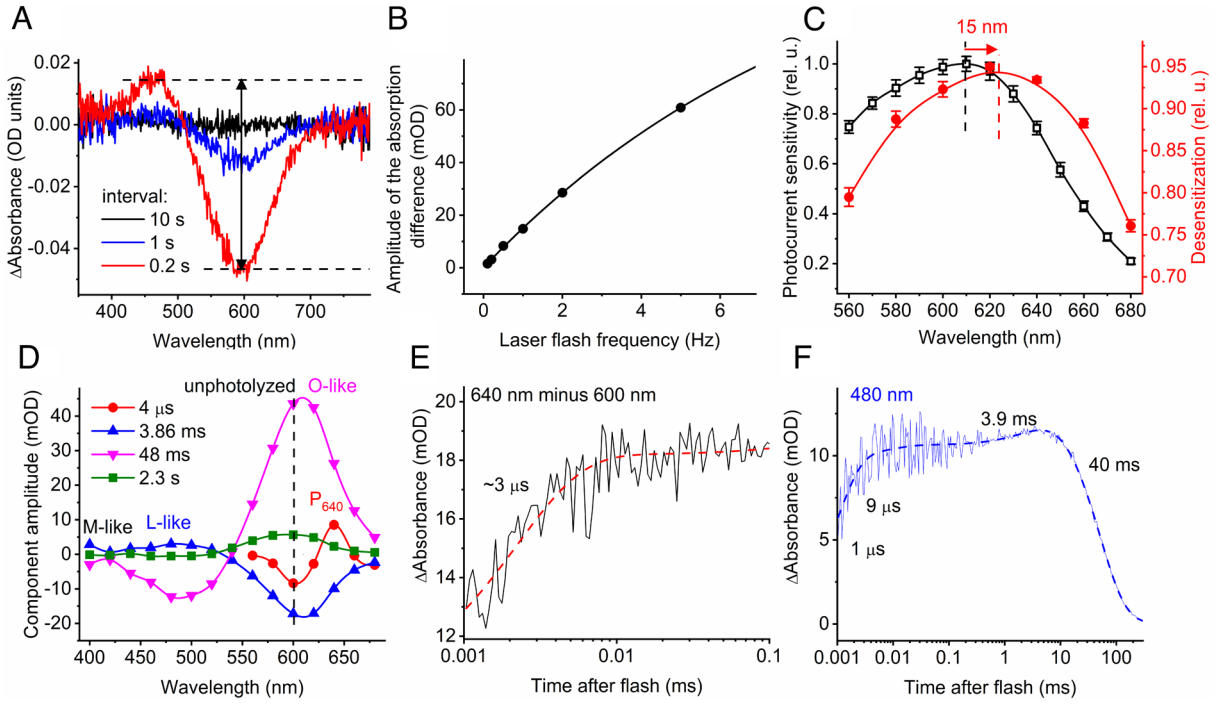

Fig. 4. Characterization of the second quantum target and the single turnover photocycle. (*A*) Difference absorption spectra of purified *Hf*ACR1 recorded after photoexcitation with 20 laser flashes (532 nm, 6 ns, 5 mJ) applied with the dark intervals of 10, 1, or 0.2 s. The arrow shows the amplitude of the absorption difference in the 0.2 s trace. (*B*) The dependence of the amplitude of the absorption difference on the laser flash frequency. (*C*) The action spectra of photocurrents (black, *Left* axis) and their desensitization (red, *Right* axis) measured as described in *Materials and Methods*. The symbols are the mean values ± SEM, n = 4 cells. (*D*) Kinetic component amplitudes derived by global fit analysis of transient absorption changes in purified *Hf*ACR1 are shown in *SI Appendix*, Fig. S2. (*E*) The time course of P_{640} revealed by subtraction of transient absorption changes at 600 nm from those at 640 nm. (*F*) The time course of the absorption changes at 480 nm reflecting the L and N intermediates.

independent of V_h (*SI Appendix*, Fig. S7) and is contributable to charge movement associated with *trans-cis* isomerization of retinal as described earlier (27).

Channel opening accelerated nearly twice upon shifting V_h 100 mV to positive values, whereas channel closing became slower to the same extent (*SI Appendix*, Fig. S8). Fig. 5*C* shows the anticorrelation between the rates of channel opening and closing. The faster the channel opened, the slower it closed. The same anticorrelation was observed not only in individual cells tested at different voltages, but also in photocurrents recorded from different cells.

Upon 0.1 Hz laser flash excitation, no reduction of the photocurrent amplitude was observed in a series of flashes (Fig. 5*D*, black filled circles), in full agreement with the absence of light-induced absorbance changes under these conditions (Fig. 2*A*, black). As expected, laser-evoked photocurrent was strongly suppressed by preillumination with red light and slowly recovered in the minute range (Fig. 5*D*, black triangles and red fitted curve). Background illumination with blue light applied after red light partially restored photocurrent (Fig. 5*D*, blue symbols). The decrease of current by red light preillumination was less than expected from the nearly full disappearance of the unphotolyzed form in purified protein (Fig. 1*A*), which indicated that 532-nm laser flashes excited L_{long} and generated photocurrent. This hypothesis was confirmed by comparing the kinetics of laser-evoked current in dark-adapted and red light preilluminated cells (Fig. 5*E*). Opening of the channel in the latter case was biphasic with τ 3- and 12-fold slower than that of the single-exponential opening in dark-adapted cells, and channel closing was faster. It means that the open state of L_{long} appears during a not yet finalized photocycle.

The channel opening of dark-adapted *Hf*ACR1 showed no temporal correlation with any single intermediate of its photocycle (Fig. 5*F*). The channel opened after a nearly full accumulation of the L-like intermediate (Fig. 5*F*, red and blue lines, respectively), but two orders of magnitude faster than accumulation of the M-like intermediate (Fig. 5*F*, black line). The kinetics of mono-exponential closing of the channel was also faster than the dissipation of either intermediate.

Discussion

Ideally, temporally precise control of membrane potential requires optogenetic tool responses that kinetically match the light stimulus, but all ChRs exhibit desensitization (reduction of photocurrents during continuous illumination). Moreover, ChR photocurrents are not restored upon application of a second light stimulus immediately after decay but only after a dark recovery period. The rates of desensitization and dark recovery vary between different ChRs (2, 24, 25). Desensitization results from accumulation of a long-lived non- or poorly conductive intermediate(s) of the photocycle, but its molecular mechanisms remain poorly understood and appear to be different in different ChRs.

In stramenopile ACRs known as MerMAIDs, strong desensitization was attributed to the formation of a long-lived M intermediate in the photocycle initiated by absorption of a single photon (24), and in *Rhodomonas* bacteriorhodopsin-like channelrhodopsins, to formation of an additional UV-absorbing intermediate (25). Desensitization in ChR2 from *Chlamydomonas reinhardtii*, the most frequently used depolarizing optogenetic tool (28), results from accumulation of an intermediate designated P_{480}. According to one model, P_{480} is formed by branching of the photocycle at the late stage (22), whereas a different model proposes its formation at an early stage in which the energy of the absorbed photon drives not only the usual all-*trans*, C = N-*anti* → 13-*cis*, C = N-*anti*

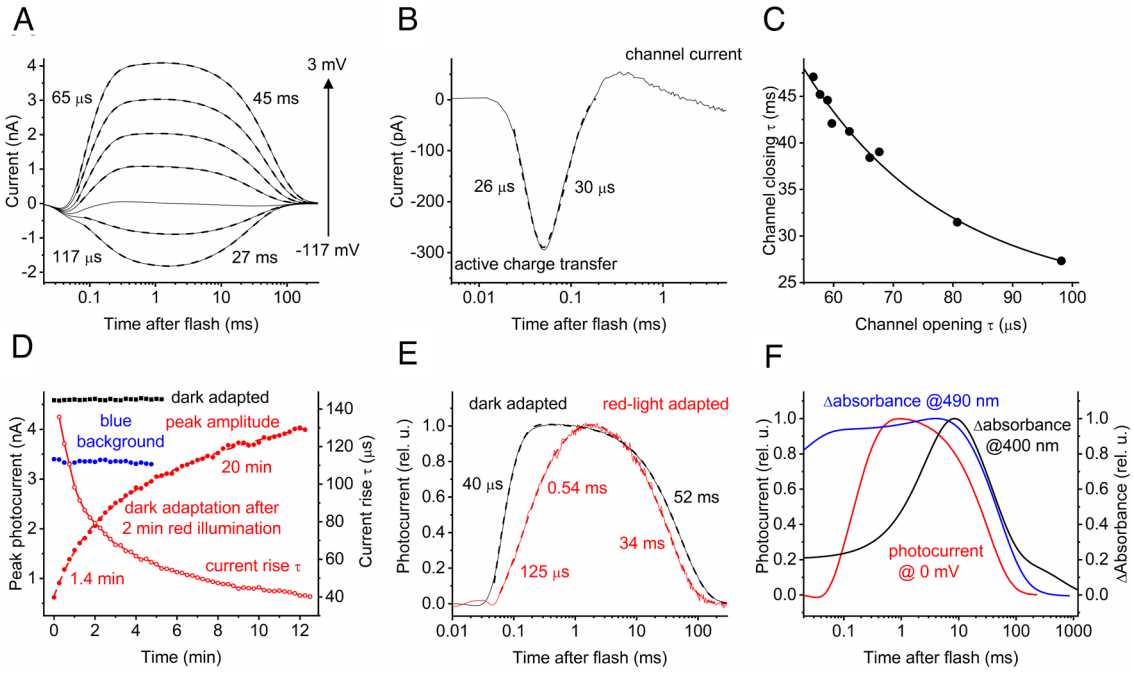

Fig. 5. Photocurrents under single-turnover conditions. (*A*) A series of photocurrent traces recorded at incremental voltages in response to laser flashes (530 nm, 6 ns, 5 mJ, 0.1 Hz). (*B*) A magnified portion of the current trace recorded at −77 mV showing active charge transfer. (*C*) The dependence of channel closing τ on the channel opening τ in the current traces recorded at different voltages. (*D*) Filled symbols, *Left* axis: Peak photocurrent amplitude recorded in response to 6-ns laser flashes (532 nm, 5 mJ, 0.05 Hz) from dark-adapted cells (black filled squares), cells preilluminated with 600-nm red light of 6 mW cm^{-2} for 60 s (red filled circles), and red light–preilluminated cells illuminated with 500-nm blue light of 4 mW cm^{-2} for 75 s (blue filled circles). Red empty circles, *Right* axis: Photocurrent rise τ in red light–preilluminated cells. (*E*) Laser flash–evoked photocurrents recorded from dark-adapted cells (black line) and cells preilluminated with 600-nm red light of 6 mW cm^{-2} for 60 s (red line). (*F*) Comparison of the laser flash–evoked photocurrent trace (red line, *Left* axis) with the time courses of the absorption changes at 490 nm (L-like and N-like intermediates) and 400 nm (an M-like intermediate) (blue and black lines, respectively, *Right* axis).

isomerization, but also all-*trans*, C = N-*anti* → 13-cis, C = N-*syn* isomerization (23). Neither model invokes absorption of the second photon as the cause of initiation of the second desensitizing photocycle. Note the lifetime of P_{480} is 10,000-fold shorter than that of the nonconductive state in RubyACRs, suggesting that the desensitization recovery process may differ.

As we report here, the RubyACRs differ in mechanism from these earlier studied examples (Fig. 6). Absorption of a single photon initiates a fast photocycle with K, L, M, and O intermediates, typical of retinal proteins (Fig. 4 *D*–*F* and *SI Appendix*, Fig. S3). During the photocycle, the channel remains open for ~50 ms (Fig. 5*E*). The cycle is completed in seconds and does not lead to the appearance of long-lived nonconductive states. However, absorption of a single quantum not only initiates the single-turnover cycle, but also leads to the appearance of an intermediate $P_{640\ in}$ ~3 µs that remains for ~100 ms, longer lived than the fast photocycle's K intermediate (Fig. 4 *B*, *D*, and *E*). The photocycles of most microbial rhodopsins contain two red-shifted intermediates: K-like and O-like (16, 18). P_{640} is unlikely to correspond to O, because O is the late intermediate that appears after L, M, and N. In contrast, formation of P_{640} takes place on the same or faster time scale as the appearance of the L-like intermediate, and far earlier than the M-like photointermediate. In addition, the peak of the fast recovery of absorption in the red spectral region is slightly red shifted from the peak of the unphotolyzed state (Fig. 4*C* and *SI Appendix*, Fig. S8), which may indicate a contribution of a more typical long-lived O-like intermediate. We conclude that P_{640} represents a late form of the K intermediate and is a critical intermediate in the desensitization process. Absorption of a second red photon by P_{640} converts the protein into an extremely long-living nonconductive state with an absorption maximum of 480 nm (L_{long}). In the dark, L_{long} slowly (>1 h) converts to an also nonconductive intermediate M_{long} that absorbs maximally at ~380 nm (Fig. 1 *C* and *D*). Full recovery of the unphotolyzed state in the dark requires several days. However, both long-lived forms are photoactive, and the unphotolyzed state can be immediately recovered from L_{long} or M_{long} by illumination with blue and UV light, respectively (Fig. 1*F*). In other words, absorption of two red photons converts *Hf*ACR1 into a bistable form. Excitation of nonconductive L_{long} opens the channel for ~35 ms (Fig. 5*E*, red trace).

The strong and long-lasting desensitization of RubyACRs reduces their utility as optogenetic tools. Our analysis of RubyACR photochemistry has revealed that the reason for this extreme

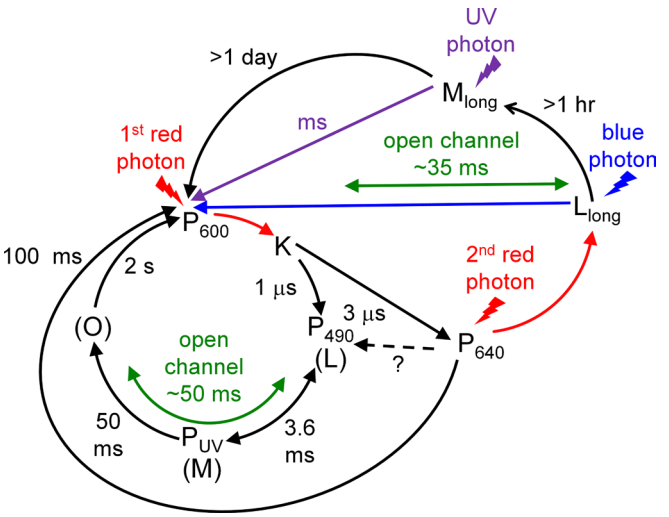

Fig. 6. A proposed scheme of RubyACR photocycle. The red, blue, and violet arrows show photoinduced conversions; the black arrows, thermal conversions. The double-headed green arrows show the lifetimes of the channel open states.

desensitization is accumulation of L_{long} and M_{long} upon absorption of a second photon. Therefore, illumination protocols that limit this accumulation are expected to decrease RubyACR desensitization in optogenetic experiments. One approach could be using trains of short light pulses instead of continuous illumination. Another approach could be alteration of red-light pulses with blue-light pulses, or using a blue-light background to restore red-light efficiency between pulses. For this second approach, to preserve the advantage of deep tissue penetration by RubyACR, the blue light would need to be delivered by a shorter route through the tissue, or for longer time. However, the efficiency of these approaches needs to be tested in neurons and may depend on a particular preparation.

Materials and Methods

HEK293 Transfection and Patch Clamp Recording. A mammalian-codon optimized DNA construct encoding the transmembrane domain of *Hf*ACR1 (GenBank accession #MT002469) was cloned into the mammalian expression vector pcDNA3.1 (Life Technologies) in-frame with an enhanced yellow fluorescent protein tag. This plasmid is available from Addgene (plasmid #161026).

HEK293 cells were transfected using the ScreenFectA transfection reagent (Waco Chemicals) and supplemented with all-*trans*-retinal (Sigma) at the 3 μM final concentration. Photocurrents were recorded 48 to 96 h after transfection in the whole-cell voltage clamp mode with an Axopatch 200B amplifier and digitized with a Digidata 1440A using pClamp 10 software (all from Molecular Devices). To mimic ionic conditions of mature neurons, the pipette solution contained (in mM): K gluconate 135, $MgCl_2$ 2, HEPES 20, pH 7.2, and the bath solution contained (in mM): NaCl 122, KCl 2, $MgCl_2$ 1, $CaCl_2$ 2, glucose 30, HEPES 25, pH 7.3. The holding voltages were corrected for liquid junction potentials calculated using the Clampex built-in calculator. Continuous light pulses were provided by a Polychrome V light source (T.I.L.L. Photonics GMBH), in combination with a mechanical shutter (Uniblitz Model LS6, Vincent Associates; half-opening time 0.5 ms). The action spectra of photocurrents were constructed by calculation of the initial slope of photocurrent recorded in response to 15-ms light pulses at the intensity <25 μW mm^{-2}, corrected for the quantum density measured at each wavelength and normalized to the maximal value. To measure the action spectrum of desensitization, 1-s light pulses at the maximal available intensities for each wavelength (4 to 8.5 mW mm^{-2}) were used. Desensitization was calculated by dividing the difference between the photocurrent value at the peak and at the end of illumination by the value at the peak. The resultant desensitization values were corrected for the quantum density measured at each wavelength and normalized to the maximal value. Laser excitation was provided by a Minilite Nd:YAG laser (532 nm, pulsewidth 6 ns, energy 5 mJ; Continuum). The current traces were logarithmically filtered using Logpro software freely available from Zenodo (29). Curve fitting was performed by Origin Pro software (OriginLab Corporation).

Expression and Purification of *Hf*ACR1 from Pichia Pastoris. The *Hf*ACR1 expression construct was fused in-frame with a C-terminal 8-His tag and subcloned into the pPIC9K vector (Invitrogen). The resultant plasmid was linearized with SalI and used to transform *P. pastoris* strain SMD1168 (*his4, pep4*) by electroporation according to the manufacturer's instructions. Resistant transformants were selected on 4 mg/mL geneticin. Transgene expression was induced by the addition of 0.5% methanol in the presence of 5 μM all-*trans* retinal. After 24 to 30 h growth, the cells were harvested and disrupted in a bead beater (BioSpec Products) as described previously (14). Membrane fragments were collected by ultracentrifugation and solubilized by incubation with 1.5% dodecyl maltoside for 1.5 h at 4 °C. The supernatant was mixed with nickel-nitrilotriacetic acid agarose beads (Thermofisher) and loaded on a column. The protein was eluted with buffer containing 300 mM imidazole, which was removed by repetitive washing using YM-10 centrifugal filters (Amicon).

Absorption Spectroscopy and Flash Photolysis. Absorption spectra of purified *Hf*ACR1 were recorded using a Cary 4000 spectrophotometer (Varian). Light-induced absorption changes were measured with a laboratory-constructed crossbeam apparatus. Excitation flashes were provided by a Minilite II Nd:YAG laser (532 nm, pulsewidth 6 ns, energy 5 mJ; Continuum). Measuring light was from a 250-W incandescent tungsten lamp combined with an McPherson monochromator (model 272, Acton). Absorption changes were detected with a Hamamatsu Photonics photomultiplier tube (model R928) combined with a second monochromator of the same type. Signals were amplified by a low-noise current amplifier (model SR445A; Stanford Research Systems) and digitized with a GaGe Octopus digitizer board (model CS8327, DynamicSignals LLC), with a maximal sampling rate of 50 MHz. Logarithmic filtration of the data was performed using the GageCon program (30). Global fit of spectral transitions was performed using the FITEXP program (31). The action spectrum of the disappearance of the initial unphotolyzed state (bleaching) shown as the red line in *SI Appendix*, Fig. S1 was obtained as follows. The sample was illuminated by monochromatic light of different wavelengths, the difference in absorption after such illumination was corrected by the light dose, and the amplitude of absorbance decrease was plotted on the graph.

Preventing Long-Lasting Desensitization and Possible Progressive Changes of Object Characteristic during Long Experiments. To avoid long-lasting desensitization for absorption and electrical measurements, samples were preilluminated with blue light before each repeated measurement. For voltage and spectral dependence, the holding potential and wavelength, respectively, were increased from minimal to maximal values and then decreased back to the minimal value, and the averaged signals were analyzed.

Statistics. The data are presented as mean ± SEM values.

Data, Materials, and Software Availability. All study data are included in the article and/or *SI Appendix*.

ACKNOWLEDGMENTS. This work was supported by the NIH Grants R35GM140838 and U01NS118288 (J.L.S.), and the Robert A. Welch Foundation Endowed Chair AU-0009 (J.L.S.).

1. E. G. Govorunova *et al.*, Cation and anion channelrhodopsins: Sequence motifs and taxonomic distribution. *mBio* **12**, e0165621 (2021).
2. E. G. Govorunova, O. A. Sineshchekov, X. Liu, R. Janz, J. L. Spudich, Natural light-gated anion channels: A family of microbial rhodopsins for advanced optogenetics. *Science* **349**, 647–650 (2015).
3. E. G. Govorunova, C. R. Cunha, O. A. Sineshchekov, J. L. Spudich, Anion channelrhodopsins for inhibitory cardiac optogenetics. *Sci. Rep.* **6**, 33530 (2016).
4. O. Tolstenkov *et al.*, Functionally asymmetric motor neurons contribute to coordinating locomotion of *Caenorhabditis elegans*. *Elife* **7**, e34997 (2018).
5. F. Mohammad *et al.*, Optogenetic inhibition of behavior with anion channelrhodopsins. *Nat. Methods* **14**, 271–274 (2017).
6. G. A. Mohamed *et al.*, Optical inhibition of larval zebrafish behaviour with anion channelrhodopsins. *BMC Biol.* **15**, 103 (2017).
7. Y. Li *et al.*, Hypothalamic circuits for predation and evasion. *Neuron* **97**, 911–924.e5 (2018).
8. A. R. Acharya *et al.*, Attenuation of hippocampal evoked potentials in vivo by activation of *Gt*ACR2, an optogenetic chloride channel. *Front. Neurosci.* **15**, 287 (2021).
9. D. E. Wilson, B. Scholl, D. Fitzpatrick, Differential tuning of excitation and inhibition shapes direction selectivity in ferret visual cortex. *Nature* **560**, 97–101 (2018).
10. A. R. Andrei *et al.*, Heterogeneous side-effects of cortical inactivation in behaving animals. *Elife* **10**, e66400 (2021).
11. Y. Zhou *et al.*, Optogenetic control of plant growth by a microbial rhodopsin. *Nat. Plants* **7**, 144–151 (2021).
12. H. Beaudry, I. Daou, A. Ribeiro-da-Silva, P. Seguela, Will optogenetics be used to treat chronic pain patients? *Pain Manag.* **7**, 269–278 (2017).
13. A. R. Ochs, T. V. Karathanos, N. A. Trayanova, P. M. Boyle, Optogenetic stimulation using anion channelrhodopsin (*Gt*ACR1) facilitates termination of reentrant arrhythmias with low light energy requirements: A computational study. *Front. Physiol.* **12**, 718622 (2021).
14. E. G. Govorunova *et al.*, RubyACRs, non-algal anion channelrhodopsins with highly red-shifted absorption. *Proc. Natl. Acad. Sci. U.S.A.* **117**, 22833–22840 (2020).
15. J. L. Spudich, C.-S. Yang, K.-H. Jung, E. N. Spudich, Retinylidene proteins: Structures and functions from archaea to humans. *Annu. Rev. Cell Dev. Biol.* **16**, 365–392 (2000).
16. O. P. Ernst *et al.*, Microbial and animal rhodopsins: Structures, functions, and molecular mechanisms. *Chem. Rev.* **114**, 126–163 (2014).
17. E. G. Govorunova, O. A. Sineshchekov, H. Li, J. L. Spudich, Microbial rhodopsins: Diversity, mechanisms, and optogenetic applications. *Annu. Rev. Biochem.* **86**, 845–872 (2017).
18. H. Kandori, Biophysics of rhodopsins and optogenetics. *Biophys. Rev.* **12**, 355–361 (2020).
19. R. H. Lozier, R. A. Bogomolni, W. Stoeckenius, Bacteriorhodopsin: A light-driven proton pump in *Halobacterium halobium*. *Biophys. J.* **15**, 955–962 (1975).
20. O. A. Sineshchekov, H. Li, E. G. Govorunova, J. L. Spudich, Photochemical reaction cycle transitions during anion channelrhodopsin gating. *Proc. Natl. Acad. Sci. U.S.A.* **113**, E1993–2000 (2016).
21. M. K. Verhoefen *et al.*, The photocycle of channelrhodopsin-2: Ultrafast reaction dynamics and subsequent reaction steps. *Chemphyschem* **11**, 3113–3122 (2010).
22. M. Saita *et al.*, Photoexcitation of the P4(480) state induces a secondary photocycle that potentially desensitizes channelrhodopsin-2. *J. Am. Chem. Soc.* **140**, 9899–9903 (2018).

23. J. Kuhne *et al.*, Unifying photocycle model for light adaptation and temporal evolution of cation conductance in channelrhodopsin-2. *Proc. Natl. Acad. Sci. U.S.A.* **116**, 9380–9389 (2019).
24. J. Oppermann *et al.*, MerMAIDs: A family of metagenomically discovered marine anion-conducting and intensely desensitizing channelrhodopsins. *Nat. Commun.* **10**, 3315 (2019).
25. O. A. Sineshchekov *et al.*, Conductance mechanisms of rapidly desensitizing cation channelrhodopsins from cryptophyte algae. *mBio* **11**, e00657-20 (2020).
26. O. A. Sineshchekov, E. G. Govorunova, H. Li, J. L. Spudich, Gating mechanisms of a natural anion channelrhodopsin. *Proc. Natl. Acad. Sci. U.S.A.* **112**, 14236–14241 (2015).
27. O. A. Sineshchekov, E. G. Govorunova, J. Wang, H. Li, J. L. Spudich, Intramolecular proton transfer in channelrhodopsins. *Biophys. J.* **104**, 807–817 (2013).
28. G. Nagel *et al.*, Channelrhodopsin-2, a directly light-gated cation-selective membrane channel. *Proc. Natl. Acad. Sci. U.S.A.* **100**, 13940–13945 (2003).
29. J. L. Spudich, LogPro (Zenodo, 2022). 10.5281/zenodo.6461999.
30. S. A. Waschuk, A. G. J. Bezerra, L. Shi, L. S. Brown, *Leptosphaeria* rhodopsin: Bacteriorhodopsin-like proton pump from a eukaryote. *Proc. Natl. Acad. Sci. U.S.A.* **102**, 6879–6883 (2005).
31. A. K. Dioumaev, Evaluation of intrinsic chemical kinetics and transient product spectra from time-resolved spectroscopic data. *Biophys. Chem.* **67**, 1–25 (1997).